Effect of current direction on the dynamics of Josephson-junction arrays

L. L. Sohn, M. S. Rzchowski, J. U. Free,* and M. Tinkham

Department of Physics and Division of Applied Sciences, Harvard University, Cambridge, Massachusetts 02138

C. J. Lobb

Center for Superconductivity Research, Department of Physics, University of Maryland, College Park, Maryland 20742

We present an extensive experimental and theoretical study of the effect that the current direction has on the dynamical properties of rf and dc current-biased overdamped Josephson-junction arrays. We show that a strong *spatial symmetry* of the array about the direction of the macroscopic current flow is necessary for arrays to show *only* integer giant Shapiro steps. If this symmetry is broken, arrays will produce *both* fractional *and* integer giant Shapiro steps. A moving-vortex model and a pendulum model are used to describe our experimental and computational results.

I. INTRODUCTION

When a single overdamped Josephson junction is both dc and rf current biased, the junction can phase lock to the rf current at voltages

$$\langle V_n \rangle = n \frac{h\nu}{2e}, \quad n = 0, 1, 2, \ldots, \tag{1}$$

where ν is the rf frequency.[1] When this phase locking occurs, we say that the junction is on its nth Shapiro step. Josephson junctions arranged in an $N \times M$ square-lattice array (where N is the number of junctions in the direction of the current flow) can also phase lock to the rf current at voltages[2]

$$\langle V_n \rangle = n \frac{N h\nu}{2}, \quad n = 0, 1, 2, \ldots. \tag{2}$$

When this collective effect occurs, i.e., when all the junctions are simultaneously on the nth Shapiro step, we say that the array is on its nth *giant* Shapiro step. In the presence of a transverse magnetic field which corresponds to a strongly commensurate number of flux quanta per plaquette, $f = p/q$ (where p and q are small integers), the array can again phase lock to the rf current but at voltages[3-6]

$$\langle V_n \rangle = n \frac{N h\nu}{q 2e},$$

$$n = 1, 2, 3, \ldots \text{ and } q = 1, 2, 3 \ldots. \tag{3}$$

For $q > 1$, these particular steps are named *fractional* giant Shapiro steps and have been attributed to the driven motion of a superlattice of field-induced vortices commensurate with the underlying array lattice.[3,5]

Recently, we found that changing the direction of the applied macroscopic current with respect to the array unit cell can greatly affect the dynamical properties of proximity-effect square-lattice Josephson-junction arrays.[7] In particular, we found that if the transport current is injected along the [11] direction of the array, the array exhibited *only* integer giant [Eq. (2)] and *not*

fractional giant [Eq. (3)] Shapiro steps.[8] We attributed this to the fact that *all* the junctions in the [11]-oriented array are directly injected with equal components of the macroscopic current (as is *not* the case for the [10]-oriented array). Through simulations, we found that this results in the entire array behaving like M coupled one-dimensional arrays.

In this paper, we present a more extensive study of the effect current direction has on the dynamical properties of proximity-effect Josephson-junction arrays. This study includes measurements made on square-lattice arrays whose macroscopic current is injected at 15° with respect to the [10] direction. These measurements show that 15° arrays also exhibit fractional giant Shapiro steps, albeit small ones. We argue that the breaking of the array's spatial symmetry in the presence of the bias current is necessary for the array to exhibit fractional giant Shapiro steps.

We also present our study of triangular-lattice arrays, arrays in which each superconducting island is surrounded by six nearest neighbors in a close-packed geometry. These particular arrays are of special interest since they are a better model than the square-lattice geometry for naturally occurring grains in samples of granular superconductor. By changing the direction of the applied macroscopic current with respect to the array, we were again able to affect the presence or absence of the fractional giant Shapiro steps in the array. A summary of our findings can be found in Table I. Finally, we use both phenomenological and analytical models to describe our results for square- and triangular-lattice arrays.

This paper is organized as follows. In Sec. II, we briefly describe our sample fabrication and measurement techniques. In Sec. III, we present our experimental results, paying particular attention to the results we obtained for the 15° square- and the triangular-lattice arrays. Section IV describes our numerical simulations of both the square- and triangular-lattice arrays. In Sec. V, we present both macroscopic and microscopic descriptions of the dynamics of square-lattice arrays, and extend them to the triangular geometry. Finally, in Sec. VI, we present our conclusions.

II. SAMPLE FABRICATION
AND MEASUREMENT TECHNIQUES

We have studied square- and triangular-lattice arrays of proximity-effect Josephson junctions in which the transport current is injected along a variety of directions. All arrays were fabricated and measured in a similar manner. A 0.3 μm thick Cu film was thermally evaporated onto a previously patterned sapphire substrate. After Ar ion etching the Cu (to clean the surface and therefore create a better interface), a 0.2 μm Nb film was sputtered onto the sample. A liftoff of the underlying photoresist then was done in order to define the edges of the array. For square-lattice arrays, Nb cross-shaped islands were patterned (and formed using SF_6 reactive-ion etching) such that macroscopic current was injected along the [10] and [11] direction of the array unit cell (see Table I). An additional array was fabricated such that the macroscopic current was injected 15° off the [10] orientation of the array unit cell (see Table I). The square-lattice arrays we studied were 10 mm long and 1 mm wide. Each square-lattice array had a lattice constant of 10 μm and junction length of 2 μm. The [10]-oriented arrays contained 1000×100 junctions, the [11]-oriented arrays 1414×141, and the 15° array, 967×97.

For the triangular-lattice arrays, Nb six-sided asterisk islands were patterned (and again, formed using SF_6 reactive-ion etching) such that the macroscopic current was injected along the [10$\bar{1}$] and [2$\bar{1}$$\bar{1}$] direction of the array unit cell (see Table I). Unlike the earlier square-lattice arrays, the differently oriented triangular-lattice arrays were fabricated on the same substrate in order to minimize fabrication inconsistencies. The lattice constant of these arrays was 16 μm. The junction length was

TABLE I. Strengths of fractional giant Shapiro steps produced by various geometries of Josephson-junction arrays. The black crosses and asterisks are Nb islands. The applied macroscopic current flows horizontally and "geometry" indicates the direction of the current with respect to the array unit cell. All array types showed integer giant Shapiro steps.

Array	Geometry	Fractional Steps
✚✚✚ ✚✚✚ ✚✚✚	[10]	Strong
✚✚✚ ✚✚✚ ✚✚✚	15°	Weak
✖✖✖ ✖✖✖ ✖✖	[11]	Absent
✳✳✳ ✳✳✳ ✳✳✳	[10$\bar{1}$]	Weak
✳✳✳ ✳✳✳	[2$\bar{1}$$\bar{1}$]	Absent

2 μm, as in the [10]-oriented square-lattice arrays. The macroscopic dimensions were 10 mm by 3 mm. While the [10$\bar{1}$]-oriented triangular-lattice array contained 722×188 junctions, the [2$\bar{1}$$\bar{1}$]-oriented array contained 625×217 junctions.

The [10], [11], and 15° square-lattice arrays exhibited normal state resistances, r_n, ranging from 2.6 to 5.0 mΩ per junction and possessed Kosterlitz-Thouless transition temperatures (T_{KT}) ranging from 1.2 to 3.3 K. The triangular-lattice arrays showed slightly different properties: r_n ranged from 1.40 to 1.67 mΩ per junction, and T_{KT} from 4.5 to 4.75 K. Using a lock-in amplifier to make four-point measurements, we characterized the arrays in terms of magnetoresistance and in terms of dynamic resistance (dV/dI) versus dc voltage or current for various external magnetic fields, rf frequencies and amplitudes, and temperatures.

III. EXPERIMENTAL RESULTS

Some of our data on the magnetoresistance of square- and triangular-lattice arrays are shown in Figs. 1(a) and 1(b). As had been reported earlier through experiments by Brown and Garland[9] and through simulations by Shih and Stroud,[10] the magnetoresistances of the two types of array lattices differ greatly. While the strongest resistance minimum (apart from f = integer) for both the square- and triangular-lattice arrays is at $f = \frac{1}{2}$, the next strongest minimum for the square-lattice array is at
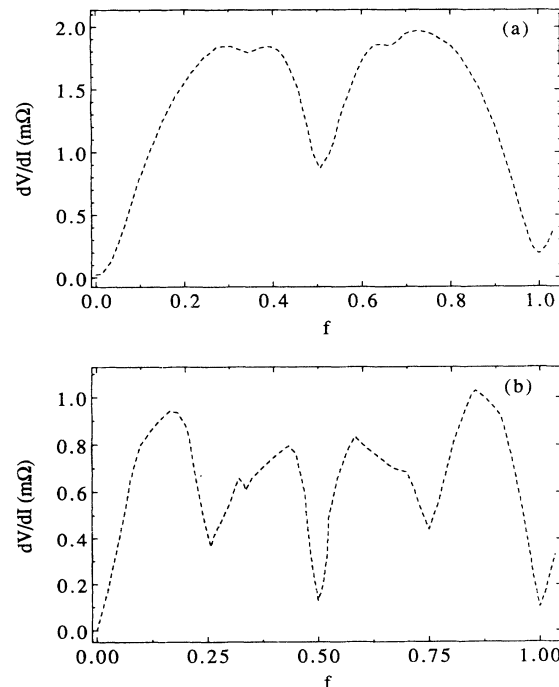

FIG. 1. Dynamic resistance vs number of flux quanta, f, per unit cell for the (a) square- and (b) triangular-lattice arrays. Data were taken at (a) $T = 2.51$ K and (b) $T = 3.97$ K. Both array lattices show strongest vortex pinning at $f = \frac{1}{2}$; however, the next strongest pinning for the square-lattice array is at $f = \frac{1}{3}$, for the triangular lattice, $f = \frac{1}{4}$.

$f = \frac{1}{3}$; for the triangular lattice, it is at $f = \frac{1}{4}$. Such resistance minima indicate pinning of the vortex superlattice. We have found that although the main features of the low-current magnetoresistance are *dependent* on the fundamental lattice of the array, these features are *independent* of the orientation of the array with respect to the transport current.[11]

As we have reported earlier,[7] both the [10]- and [11]-oriented square-lattice arrays exhibit integer giant Shapiro steps at voltages corresponding to Eq. (2), but only the [10]-oriented and not the [11]-oriented arrays display fractional giant Shapiro steps for commensurate f values at voltages corresponding to Eq. (3). In our present study, we find that both integer and fractional giant Shapiro steps appear in the 15° array (see Fig. 2), but the fractional step, $n/q = 1/2$, in the 15° array is quite weak, as determined by the minimum dynamic resistance; fractional giant Shapiro steps of $n/q > 3/2$ are nearly nonexistent. This is in striking contrast to the [10]-oriented arrays,[12] in which we observed strong fractional giant Shapiro steps for $n/q > 3/2$. Subharmonic steps, which were so prevalent in our [10]-oriented arrays at rf frequencies $\Omega > 3$ (where $\Omega = h\nu/2ei_c r_n$, and i_c and r_n are the critical current and normal state resistance per junction, respectively[7]), also appear in the 15° array, albeit weakly, for $0.18 < \Omega < 1.24$.

The general dynamical properties of the triangular-lattice arrays have many parallels to those of the square-lattice ones. In Fig. 3(a), we see that, as in the case of the [10]-oriented square-lattice arrays, the [$10\bar{1}$]-oriented triangular-lattice arrays exhibit both integer and fractional giant Shapiro steps[13] at voltages corresponding to Eqs. (2) and (3). In Fig. 3(b), we see that the [$2\bar{1}\bar{1}$]-oriented triangular-lattice arrays, like the [11]-oriented square-lattice arrays, show only integer giant [Eq. (2)] Shapiro steps. One remarkable feature which is unique to the [$2\bar{1}\bar{1}$]-oriented triangular-lattice arrays is that the even
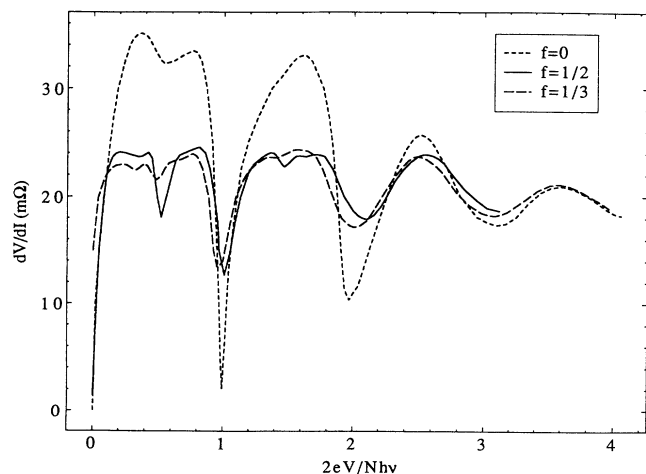

FIG. 2. Dynamic resistance vs normalized voltage for the 15° square-lattice array in the presence of perpendicular magnetic fields corresponding to $f = 0$, $\frac{1}{2}$, and $\frac{1}{3}$. Data were taken at $T = 2.52$ K and rf frequency $\nu = 3.5$ Mhz ($\Omega = h\nu/2ei_c r_n = 0.41$).
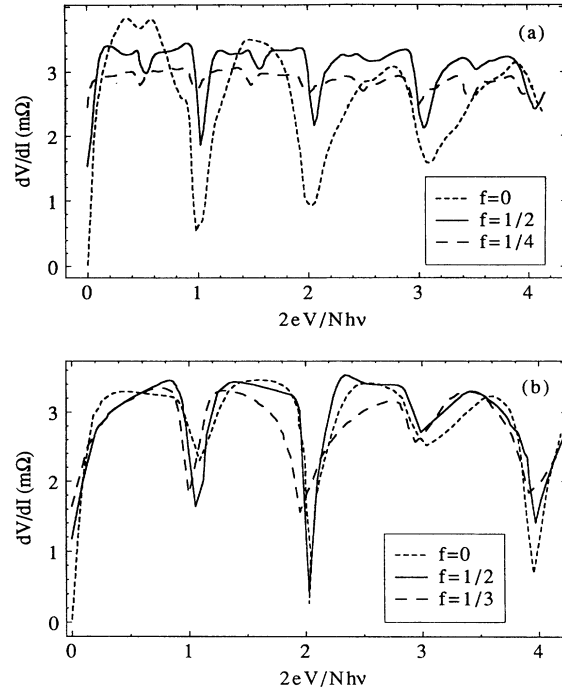

FIG. 3. Dynamic resistance vs normalized voltage for the (a) [$10\bar{1}$]-oriented and (b) [$2\bar{1}\bar{1}$]-oriented triangular-lattice arrays in the presence of perpendicular magnetic fields corresponding to $f = 0$, $\frac{1}{2}$, $\frac{1}{3}$, and $\frac{1}{4}$. (a) $T = 3.40$ K and rf frequency $\nu = 0.9$ Mhz ($\Omega = h\nu/2ei_c r_n = 0.33$). (b) $T = 3.61$ K and rf frequency $\nu = 0.7$ Mhz ($\Omega = h\nu/2ei_c r_n = 0.96$). Only the [$10\bar{1}$] case shows fractional giant Shapiro steps. Integer giant Shapiro steps in the [$2\bar{1}\bar{1}$] case alternate in strength, the even steps being stronger than the odd ones.

integer steps are much stronger than the odd ones. We have found that this unusual behavior is both field- and frequency-independent.

A summary of our results can be found in Table I. Briefly, we have found that the [10]-oriented and 15° square- and [$10\bar{1}$]-oriented triangular-lattice arrays produce *both* integer *and* fractional giant Shapiro steps. The [11]-oriented square- and [$2\bar{1}\bar{1}$]-oriented triangular-lattice arrays, however, produce *only* integer giant Shapiro steps.

IV. NUMERICAL SIMULATIONS

The RCSJ model[14] is often used to describe rf current-biased single Josephson junctions.[15] This model assumes that a Josephson junction is a parallel combination of a resistor r_n, a capacitor C, and a nonlinear Josephson element with critical current i_c. The equation of motion for this system when it is current biased is

$$\frac{\hbar C}{2e}\frac{d^2\gamma}{dt^2} + \frac{\hbar}{2er_n}\frac{d\gamma}{dt} + i_c\sin\gamma = i_{dc} + i_{rf}\sin(\omega t) , \quad (4)$$

where γ is the gauge-invariant phase difference between the two superconducting islands that make up the junction, i_{dc} and i_{rf} are the applied dc and rf current per junction, and i_c is the critical current of the junction. In the

overdamped limit $[\beta_c = (2e/\hbar)i_c r_n^2 C \ll 1]$, Eq. (4) reduces to a first-order differential equation.

In this section, we study both square- and triangular-lattice *arrays* of *overdamped* Josephson junctions. Rzchowski, Sohn, and Tinkham[16] have shown that the dynamics of an entire [10]-oriented square-lattice array at $f = \frac{1}{2}$ can be modeled with a 2×2 unit cell of the array. In Sec. IV A, we present our analysis of a 2×2 unit cell of the [11]-oriented square-lattice array at $f = \frac{1}{2}$. This analysis centers on the detailed response of the gauge-invariant phase difference across each junction in the 2×2 cell. In Secs. IV B and IV C, we extend this "microscopic" model to the unit cells of the [10$\overline{1}$]-oriented and [2$\overline{1}$ $\overline{1}$]-oriented triangular-lattice arrays, respectively, and describe our results.

A. The 2×2 unit cell of the [11]-oriented array

As has been previously discussed,[7] the [11]-oriented square-lattice array at $f = \frac{1}{2}$ can be described as a 2×2 unit cell. Following Rzchowski *et al.*,[16] we demand that the superlattice unit cell carry a net current equal to the external drive current. For the [11] geometry, we model this as equal current flows of $I_{\text{tot}}/2 = i_{\text{dc}} + i_{\text{rf}} \sin(\omega t)$ where I_{tot} is the applied current per node (normalized to the single-junction critical current, i_c), in the orthogonal [10] and [01] directions in the cell (see Fig. 4). If we satisfy fluxoid quantization and total current conservation at the central node, we can write the following equations,

$$\alpha + \gamma + \beta' + \beta = \pi \pmod{2\pi} , \tag{5a}$$

$$\frac{d\beta'}{d\tau} + \sin\beta' - \frac{d\beta}{d\tau} - \sin\beta = \frac{I_{\text{tot}}}{2} , \tag{5b}$$

$$\frac{d\gamma}{d\tau} + \sin\gamma - \frac{d\alpha}{d\tau} - \sin\alpha = \frac{I_{\text{tot}}}{2} , \tag{5c}$$

$$\frac{d\gamma}{d\tau} + \frac{d\alpha}{d\tau} + \sin\gamma + \sin\alpha - \frac{d\beta}{d\tau} - \frac{d\beta'}{d\tau} - \sin\beta - \sin\beta' = 0 , \tag{5d}$$

where α, β, β', and γ are the gauge-invariant phase differences as denoted in Fig. 4, $\tau = (2ei_c r_n/\hbar)t$, and $I_{\text{tot}} = I_{\text{dc}} + I_{\text{rf}} \sin(\omega t)$ is the applied dc and rf current per node. Making the following substitutions, $x = (\gamma - \alpha)/2$, $y = (\gamma + \alpha)/2$, $u = (\beta - \beta')/2$, and $v = (\beta + \beta')/2$, the above equations become

$$\frac{dx}{d\tau} + \cos y \, \sin x = \frac{I_{\text{tot}}}{4} , \tag{6a}$$

$$-\frac{du}{d\tau} - \sin y \, \sin u = \frac{I_{\text{tot}}}{4} , \tag{6b}$$

$$2\frac{dy}{d\tau} + \sin y \, \cos x - \cos y \, \cos u = 0 . \tag{6c}$$

If we numerically solve Eq. (6), we obtain *I-V* curves which show only integer giant Shapiro steps. In addition, we learn that $dy/d\tau = 0$. Using this fact, we find that we can reproduce the equation derived from our simulations in a previous paper,[7] namely
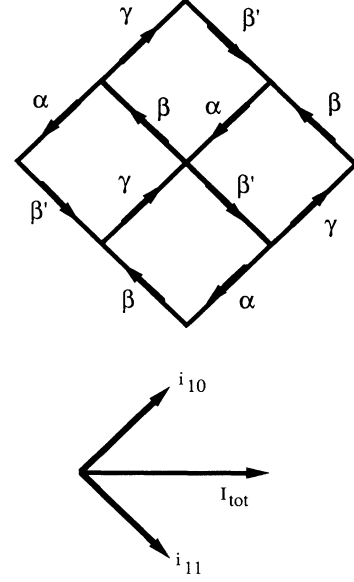

FIG. 4. 2×2 unit cell of the [11]-oriented square-lattice array. The gauge-invariant phase differences of the individual junctions are as indicated. I_{tot} is the applied current per node while i_{10} and i_{11} are the components of I_{tot} in the [10]-oriented and [11]-oriented array lattice direction. Both i_{10} and i_{11} are assumed to be $I_{\text{tot}}/2$.

$$\frac{d\zeta}{d\tau} + \frac{1}{\sqrt{2}} \sin\zeta = \frac{I_{\text{tot}}}{2} , \tag{7}$$

where $\zeta = \gamma - \pi/4$. In order to derive Eq. (7), we had previously assumed that the voltages across the junctions in a plaquette were equal to one another.[7] The numerical solution to Eq. (6) shows us that this assumption is correct.

We comment again[7] that Eq. (7) is equivalent to an equation of motion for a single overdamped Josephson junction. Renne and Polder[17] have analytically shown that these junctions produce only integer Shapiro steps. It follows then that [11]-oriented arrays produce only integer steps as well.

The analysis we have just outlined can be used only for cases in which the square-lattice array can be described by a periodically repeated 2×2 unit cell. Presently, we believe that only the [10]-oriented and [11]-oriented arrays are able to satisfy this requirement. The size of the superlattice cell in the presence of a drive current at $f = \frac{1}{2}$ for intermediate angle arrays, such as the 15° array we experimentally studied, is not known at this time. Large scale simulations are needed to determine this and to understand the finer details of these intermediate arrays.

B. The [10$\overline{1}$]-oriented array unit cell

Like the [10]-oriented square-lattice array, the [10$\overline{1}$]-oriented triangular-lattice array produces both integer and fractional giant Shapiro steps. Satisfying fluxoid quantization, current conservation, and net current flow,

we can write the following equations for the $[10\bar{1}]$-oriented array unit cell when $f = \frac{1}{2}$:

$$\alpha + \beta + \gamma = \pi \quad (\bmod 2\pi) , \tag{8a}$$

$$\frac{d\gamma}{d\tau} - \frac{d\alpha}{d\tau} + \sin\gamma - \sin\alpha = I_{tot} , \tag{8b}$$

$$\frac{d\gamma}{d\tau} + \frac{d\alpha}{d\tau} + \sin\gamma + \sin\alpha - \frac{d\beta}{d\tau} - \sin\beta = 0 , \tag{8c}$$

where α, β, and γ are the gauge-invariant phase differences denoted in Fig. 5(a). If we let $x = (\gamma - \alpha)/2$ and $y = (\gamma + \alpha)/2$, Eq. (8) becomes

$$2\frac{dx}{d\tau} + 2\cos y \, \sin x = I_{tot} , \tag{9a}$$

$$2\frac{dy}{d\tau} - \frac{1}{2}\sin 2y + \sin y \, \cos x = 0 . \tag{9b}$$

Numerically solving Eq. (9) for a variety of rf powers, we obtain I-V curves which show both integer and fractional giant Shapiro steps. A plot of the stepwidth versus rf power is shown in Fig. 5(b). The general features of Fig.
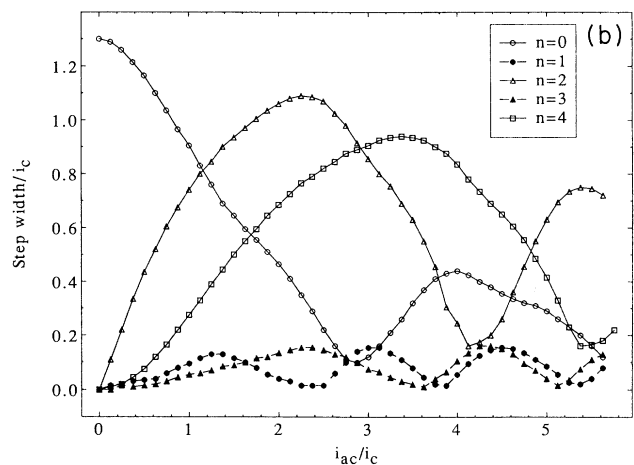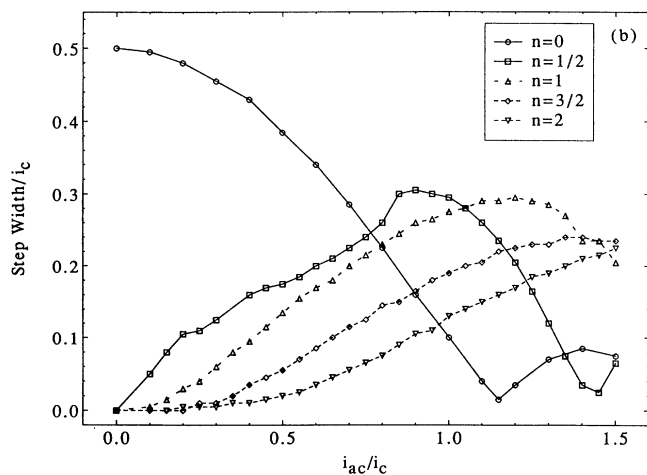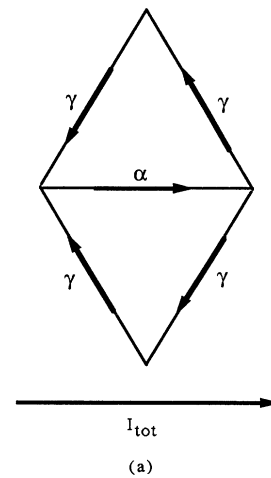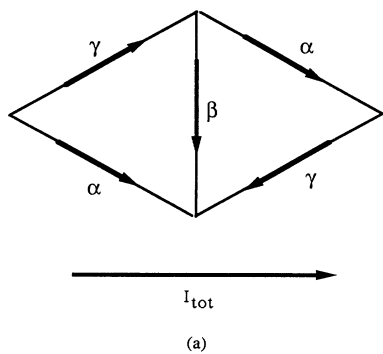
5(b), namely an oscillatory behavior similar to that of a single junction and a decrease in stepwidth with an increase in step number, are similar to those found in the stepwidth versus rf power of the [10]-oriented square-lattice array.[16]

C. The $[2\bar{1}\,\bar{1}]$-oriented array unit cell

We have simulated a $[2\bar{1}\,\bar{1}]$ triangular-lattice unit cell, such as the one shown in Fig. 6(a). Based on our knowledge of the phase evolution of the junctions in the [11]-oriented square-lattice array on an integer step at $f = \frac{1}{2}$ and at low rf frequencies,[7] we make the assumption that the phase differences of the diagonal junctions, denoted as γ in Fig. 6(a), are equal. Because the sum of the total current is conserved at each node and because fluxoid quantization requires $2\gamma - \alpha = 2\pi f$, then, for

(a)

(b)

FIG. 5. (a) Diagram of the unit cell in the $[10\bar{1}]$-oriented triangular-lattice array. The gauge-invariant phase differences of the individual junctions are as indicated. I_{tot} is again the applied current per node. (b) Simulated stepwidth vs rf power for the $[10\bar{1}]$-oriented triangular-lattice array at $f = \frac{1}{2}$. Oscillatory behavior and a decrease in stepwidth with an increase in step number are similar to single-junction behavior.

(a)

(b)

FIG. 6. (a) Diagram of the unit cell in the $[2\bar{1}\,\bar{1}]$-oriented triangular-lattice array. The gauge-invariant phase differences of the individual junctions are as indicated. Again, I_{tot} is the applied current per node. (b) Stimulated stepwidth vs rf power for the $[2\bar{1}\,\bar{1}]$-oriented triangular-lattice array at $f = 0$. Odd steps are smaller than even steps agreeing with experimental results. Even steps never go to zero.

$f = 0$, we obtain the equation

$$2\frac{d\alpha}{d\tau} + 2\sin\frac{\alpha}{2} + \sin\alpha = I_{\text{tot}} \ . \tag{10a}$$

If $f = \frac{1}{2}$, Eq. (10a) is replaced by

$$2\frac{d\alpha}{d\tau} + 2\cos\frac{\alpha}{2} + \sin\alpha = I_{\text{tot}} \ . \tag{10b}$$

Numerically solving Eq. (10a), we obtain I-V curves which show *only* integer giant Shapiro steps. Interestingly, identical I-V curves are obtained when solving Eq. (10b). Using the I-V curves we obtained, we plotted the stepwidth versus rf power. In Fig. 6(b), we show such a plot for $f = 0$ and $\Omega = 0.5$. Here we see that, as in our experimental results, the odd steps are indeed smaller than the even ones. Interestingly, the widths of the even steps never go to zero for any rf power.

V. DISCUSSION

Our experimental results and simulations show that the macroscopic current direction plays an important role in the observed step structure of square- and triangular-lattice arrays. In the systems we have studied, we found that the [10]-oriented square- and [10$\overline{1}$]-oriented triangular-lattice arrays produce strong fractional giant Shapiro steps. These arrays have junctions which are perpendicular to the transport current and hence do not carry any component of the external current. In contrast, we found that the [11]-oriented square- and [2$\overline{1}$$\overline{1}$]-oriented triangular-lattice arrays produce only integer giant Shapiro steps. All the junctions in these arrays carry some component of the external current. More importantly, however, a strong *spatial symmetry* of the array unit cell about the direction of the macroscopic current flow exists in these particular arrays. This results in the entire array being mathematically reducible to a single junction for $f = \frac{1}{2}$. The 15° array is an intermediate case, as we have found that this array produces weak fractional giant Shapiro steps. Like the [11]-oriented and [2$\overline{1}$$\overline{1}$]-oriented arrays, all of the array's junctions carry some component of the external current; however, unlike the [11]-oriented and [2$\overline{1}$$\overline{1}$]-oriented arrays, the spatial symmetry of the unit cell about the direction of the macroscopic current flow no longer exists.

Summarizing, we have found that transport current flows which retain a strong spatial symmetry in the array produce *only* integer giant Shapiro steps. When this spatial symmetry is broken, both integer *and* fractional giant Shapiro steps are observed. From our study of the square-lattice arrays, we observe that the widths of the fractional steps vary as a function of the angle of current injection. The maximum fractional stepwidth occurs when there are junctions in the array that are perpendicular to the transport current and correspondingly do not carry any component of the external current.

In the following sections, we present two models which describe the dynamical properties of proximity-effect Josephson-junction arrays.

A. The moving-vortex model

The behavior of [10] proximity-effect Josephson-junction arrays has been described in terms of the driven motion of a superlattice of field-induced vortices commensurate with the underlying array lattice.[3-6] For example, when $f = \frac{1}{2}$, the 2×2 vortex superlattice moves one array unit cell in a direction perpendicular to the transport current after one rf cycle. This motion leads to each junction in the array having an average phase slip of π per rf cycle. From the Josephson voltage relationship,[18]

$$\langle V \rangle = \frac{\hbar}{2e}\left\langle \frac{d\gamma}{dt} \right\rangle \ , \tag{11}$$

it follows that the average voltage across the entire array is

$$\langle V \rangle = N\frac{\hbar\nu}{2e}\pi = \frac{N}{2}\frac{h\nu}{2e} \ , \tag{12}$$

which is Eq. (3) with $n = 1$ and $q = 2$.

There is some ambiguity involved, however, in using the vortex model when $f = \frac{1}{2}$. This happens because every plaquette is occupied by a circulating current, so it is not completely clear whether to count clockwise currents, counterclockwise currents, or both as "vortices." Nonetheless, we have found that the vortex model is a useful *phenomenological* description. The basic *assumptions* are that the overall macroscopic motion of the vortices is perpendicular to the external current direction, and that each junction will undergo a phase slip of 2π in the time it takes for the driven vortices to return to their original configuration. (A more precise, but less intuitive, model[19] is presented in the next section.)

Consider first [11]-oriented square arrays. In this case, the overall macroscopic motion of the vortices is in the direction of the Lorentz force and toward the *next-nearest-neighbor* cells (see Fig. 7). This motion leads to a phase slippage of 2π per junction per rf cycle, or, from Eq. (11),

$$\langle V \rangle = N\frac{\hbar\nu}{2e}2\pi = N\frac{h\nu}{2e} \ . \tag{13}$$

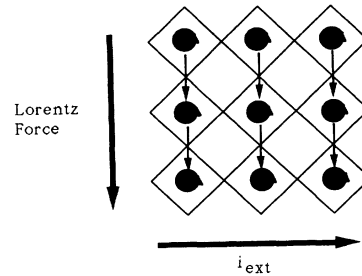Equation (13) says that the lowest voltage step is an in-

FIG. 7. Vortex configuration in the [11]-oriented square-lattice array at $f = \frac{1}{2}$. Large vertical arrow indicates the direction of the Lorentz force resulting from i_{ext}. Small arrows indicate macroscopic motion of vortices during one rf cycle on the $n/q = 1$ step.

teger step.

For any other field, $f = p/q$, the macroscopic motion of the vortices is again in the direction of the Lorentz force and toward the next-nearest-neighbor plaquettes. Each junction correspondingly phase slips $2\pi n$ per rf cycle and consequently, fractional giant Shapiro steps are not produced.

The vortex model can also be used to describe the results we have obtained for the 15° square-lattice array. In this orientation, the Lorentz force directs the vortices into the nearest-neighbor plaquette rather than the next-nearest-neighbor one. Therefore, fractional giant Shapiro steps can occur in this type of oriented array.

As we have stated previously, the experimental results we have obtained for the square- and triangular-lattice arrays are very similar. Like the [10]-oriented square-lattice array, the [$10\bar{1}$]-oriented triangular-lattice array exhibits fractional steps at voltages corresponding to Eq. (3). In Fig. 8(a) we have drawn the $f = \frac{1}{2}$ state of the [$10\bar{1}$]-oriented array. Here we see that the macroscopic motion of the vortices is toward the nearest-neighbor plaquette. Thus, the junctions in the array can slip $2\pi n/q$
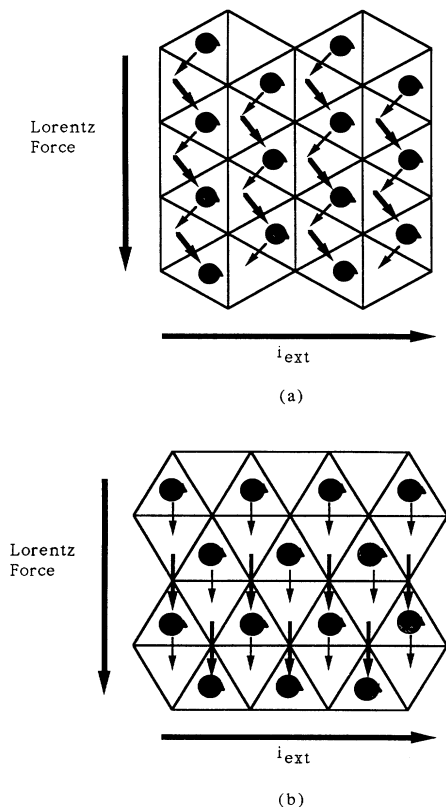
FIG. 8. Vortex configuration in the (a) [$10\bar{1}$]-oriented and (b) [$2\bar{1}\bar{1}$]-oriented triangular-lattice array at $f = \frac{1}{2}$. Again, large vertical arrow indicates the direction of the Lorentz force resulting from i_{ext}. For (a), arrows indicate macroscopic motion of vortices during 2 subsequent rf cycles on the $n/q = 1/2$ step. While the light arrows indicate vortex motion during one rf cycle, the heavy arrows indicate vortex motion during a subsequent rf cycle. For (b), light and heavy arrows show two possible vortex motions occuring sequentially in one rf cycle.

per rf cycle and correspondingly produce fractional giant Shapiro steps.

The [$2\bar{1}\bar{1}$]-oriented triangular-lattice array is the most interesting of all the arrays we have studied. In Fig. 8(b) we have drawn the $f = \frac{1}{2}$ state of this array and have indicated by arrows the macroscopic motion of the vortices. Note that under the influence of the Lorentz force, there are really two different types of vortex motion in the array. One macroscopic motion, denoted by the single arrows in the figure, consists of overcoming the low energy barrier[20] of the egg-carton potential and entering the *nearest*-neighbor plaquette. The other, denoted by the heavy-set arrows, consists of overcoming the *high* energy barrier of the egg-carton potential and entering the *next*-nearest-neighbor plaquette. A plausible scenario, then, would be for the vortices to undergo the two types of motion on successive rf cycles. It would thus appear that an $n/q = 1/2$ step would occur in the array. Based on our experiments and simulations, we know that such a step does not. We deduce that a necessary condition for a step to appear in the array is that, just as in the [10]- and [11]-oriented-array case, the vortex motion(s) on a step must be identical for each rf cycle. This means that the vortices in the [$2\bar{1}\bar{1}$]-oriented array must undergo the two different types of motion we have just outlined in each rf cycle. Hence, the array phase slips $2\pi Nn$ per rf cycle and only integer giant Shapiro steps are produced.

As we have stated previously, changing the macroscopic current direction does not affect the general features of
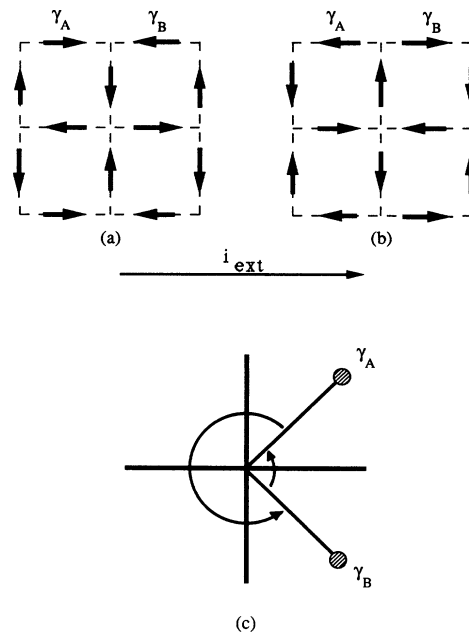
FIG. 9. Gauge-invariant phase differences, γ, for junctions in a 2×2 unit cell on the $n/q = 1/2$ step at the (a) beginning and (b) end of an rf cycle in the [10]-oriented array at $f = \frac{1}{2}$. Arrows indicate the direction of the supercurrents. The motion of γ_A and γ_B over the same time period is shown in the "pendulum" diagram (c). At the end of one rf cycle, the pendula have interchanged positions; γ_A has advanced $3\pi/2$ while γ_B has advanced by $\pi/2$.

the magnetoresistance of square- and triangular-lattice arrays, although it does affect the rf response of the individual arrays. The field modulation in a magnetoresistance measurement comes from the fact that the resistance, R, is a function of $T/T_c(f)$, which in turn is a function of field, *not* current. When we apply a small current, regardless of its direction with respect to the array, the wells in the egg-carton potential tilt slightly. Thermal fluctuations lead to the unpinning of the vortices and to the subsequent creation of a small voltage across the array. In an rf experiment, we are driving the system very hard, literally dragging the vortices from well to well. Therefore, current direction should and does play an important role in the outcome of these types of experiments.

The moving-vortex model is only a phenomenological model which explains in general terms why fractional giant Shapiro steps can or cannot exist in certain oriented arrays. However, we have been unable to explain, in context of this model, the detailed motion of how the vortices are able to by-pass the high energy barrier of the array lattice and move into the next-nearest-neighbor cell.[21] In addition, we have not been able to even qualitatively explain stepwidths using this model. In the section below, we take an entirely different approach towards explaining the presence or absence of fractional giant Shapiro steps in Josephson-junction arrays. This approach centers on examining the individual junctions in an array unit cell and applying Kirchhoff's voltage law.

B. The pendulum model

The equation of motion for a single Josephson junction [Eq. (4)] is identical to that of a damped driven pendulum with mass $\propto C$, damping $\propto 1/R$, and with constant and ac applied torques. In an array, the equations are coupled, via Kirchhoff's laws, and an array becomes equivalent to a network of coupled pendula. Thus, representing the gauge-invariant phase differences, γ_{ij}, where i and j are the ith and jth island in the array as pendula, is a pictorial and quantitative description of the dynamical properties of the array.[19]

When driven by an rf current with frequency ν, a single junction can phase lock to the rf current. When the junction is overdamped, γ swings around a total of $2\pi n$ in one rf cycle. If $d\gamma/dt$ equals $2\pi n\nu$ as we have indicated, Eq. (11) transforms into the equation of an integer Shapiro step [Eq. (1)].

The above model has been successfully applied to the [10]-oriented square-lattice array.[19] For $f=0$, the junctions parallel to the direction of the transport current act like isolated Josephson junctions and the perpendicular junctions play no role in the array. Equation (2) is obtained by considering N γ's swinging $2\pi n$ times per rf cycle.

For the $f=\frac{1}{2}$ state, the pendulum model must be applied to a 2×2 unit cell.[19] In Figs. 9(a) and 9(b), we have drawn two alternative versions of the $f=\frac{1}{2}$ ground state of such a cell. We take the phase differences, denoted as γ_A and γ_B, of the junctions parallel to the external current to be equal to $\pm\pi/4$ [the array's ground state at

$f=\frac{1}{2}$ (Ref. 22)] at the beginning of the rf cycle. When i_{ext} is applied in the direction shown in the figure, it winds γ_A and γ_B counterclockwise, γ_A by $3\pi/2$ and γ_B by $\pi/2$,[4] in one rf cycle [see Fig. 9(c)] such that the cell is now in the other $f=\frac{1}{2}$ ground state shown in Fig. 9(b). In the following rf cycle, the external current, i_{ext}, again winds γ_A and γ_B counterclockwise: this time γ_A by $\pi/2$ and γ_B by $3\pi/2$. Since half of the junctions in the array act like junction A and the other half act like junction B, we obtain an average phase slip of π per rf cycle per junction. Equation (3) is thus obtained.

For the [11]-oriented square-lattice array in the $f=0$ case, every junction is directly and equally injected with the transport current. Thus, all junctions in the array act like a single Josephson junction and will correspondingly phase slip $2\pi n$ per rf cycle. Again, we see that we have obtained Eq. (2).

For $f=\frac{1}{2}$, we look at a particular plaquette in the array. Figure 10(a) shows a plaquette with the direction of the transport current as indicated. We see in this figure that there are two different paths by which current travels across the [11]-oriented array. By Kirchhoff's voltage law, $V_A + V_B = V_C + V_D$. This additional constraint forces $\gamma_A + \gamma_B$ to rotate rigidly with $\gamma_D + \gamma_C$ by 2π per junction per rf cycle as shown in Fig. 10(b).[23] (Our simulations show that at low rf frequencies the array remains in the staircase state. By definition this means that $\gamma_A = \gamma_B$ and is $\pi/2$ out of phase with $\gamma_D = \gamma_C$).

The results we have obtained from studying the triangular-lattice array can also be explained using the pendulum model. As in the [10]-oriented square-lattice
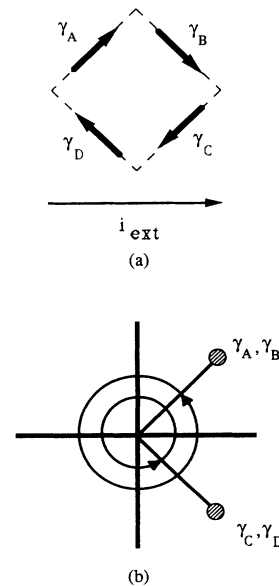

(a)

(b)

FIG. 10. (a) Gauge-invariant phase differences, γ, for junctions in a unit cell on the $n=1$ step in the [11]-oriented square-lattice array at $f=\frac{1}{2}$. Arrows indicate direction of the supercurrent. (b) The motion of γ_A and γ_B over the same time is shown in the "pendulum" diagram (c). Unlike in the [10] case, in the [11] case, each pendulum has advanced by 2π at the end of one rf cycle.

case, in the [$10\bar{1}$]-oriented triangular lattice, we find that the gauge-invariant phases are not forced to be locked together and move at some fixed rate per rf cycle in order to satisfy Kirchhoff's voltage law. The perpendicular junctions allow the other junctions to rotate more freely. Therefore, the phases can evolve such that fractional steps can exist in this type of an array.

In the [$2\bar{1}\,\bar{1}$]-oriented triangular-lattice array, we see that the array really has two types of junctions: straight-feed-through junctions, A, and diagonal ones, B and C, as shown in Fig. 11(a). By Kirchhoff's voltage law, we see that γ_A must move *twice* as fast as γ_B and γ_C per rf cycle. Thus, while junctions B and C are on their first giant Shapiro step, junction A is already on its second step [see Fig. 11(b)]. This corresponds nicely to the two-vortex motion we described in the preceding section for this type of an array; the motion the vortices undergo to travel into the next-nearest-neighbor cell corresponds to the phase evolution of junctions B and C. The motion the vortices undergo to travel into the nearest-neighbor cell corresponds to the phase evolution of junction A. Based on our analysis of the [11]-oriented square-lattice case, we propose that Kirchhoff's voltage law and the absence of perpendicular junctions again constrain the evolution of the gauge-invariant phase differences per rf cycle such that the only periodic solution is one in which the phases of the junctions rotate in multiples of 2π per rf cycle. Thus, only integer giant Shapiro steps are produced by the [$2\bar{1}\,\bar{1}$]-oriented triangular-lattice array.

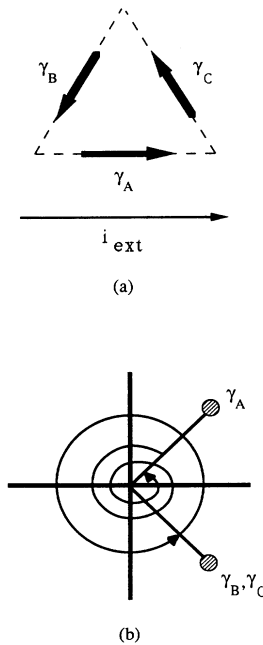The alternating step widths produced by the [$2\bar{1}\,\bar{1}$]-

FIG. 11. (a) Gauge-invariant phase differences, γ, for a plaquette in the [$2\bar{1}\,\bar{1}$]-oriented triangular-lattice array at $f = \frac{1}{2}$. Arrows again indicate the direction of the supercurrent. (b) By Kirchhoff's voltage law, $V_A = V_B + V_C$ and accordingly, γ_A must rotate $4\pi n$ per rf cycle while γ_B and γ_C each rotate $2\pi n$ per rf cycle on the nth giant Shapiro step.

oriented triangular-lattice array can be accounted for by examining Eq. (9). In this equation, we see that the $\sin(\alpha/2)$ term, the term describing the diagonal junctions, contributes to *only* the even harmonics of the time-dependent voltage since its fundamental period is $4\pi n$. The term describing the straight-feed-through junctions, $\sin(\alpha)$, contributes to *both* the even *and* odd harmonics of the time-dependent voltage as its fundamental period is $2\pi n$.[24] When the array is on an odd step, only the straight-feed-through junctions are on the step; the diagonal ones still have not locked to the rf frequency and are therefore not on a step. When the array is on an even step, however, *all* the junctions are on a step, although *not* on the *same* step. As a result, the even steps are much wider than the odd ones, and do not go to zero width because the two steps go to zero for different power levels.

We stress that because of the perpendicular junctions in the [10]-oriented square- and [$10\bar{1}$]-oriented triangular-lattice arrays, the phase differences of the other junctions are *not* tightly locked together and therefore do not have to rotate at the same rate each rf cycle. Consequently, fractional giant Shapiro steps can be produced by the array. Contrast this to the [11]-oriented square- and [$2\bar{1}\,\bar{1}$]-oriented triangular-lattice arrays in which there are no perpendicular junctions. In this case, the phase differences of the junctions are locked together and must phase slip at the same rate each rf cycle, so that the only periodic solution is one in which integer giant Shapiro steps are produced.

VI. CONCLUSION

In the course of our study, we have seen the importance of current direction on the dynamics of proximity-effect Josephson-junction arrays. When the spatial symmetry of the array is maintained in the presence of current flow, *only* integer giant Shapiro steps [Eq. (2)] are produced. The [11]-oriented square- and [$2\bar{1}\,\bar{1}$]-oriented triangular-lattice arrays we studied showed such a spatial symmetry, and indeed, these arrays produced only integer giant Shapiro steps. If, however, this spatial symmetry is broken, both integer giant [Eq. (2)] *and* fractional giant [Eq. (3)] Shapiro steps are produced. In our experiments, the bias current broke the spatial symmetry of the [10]-oriented and 15° square- and [$10\bar{1}$]-oriented triangular-lattice arrays. These arrays produced integer and fractional giant Shapiro steps.

The exact relationship between decreasing fractional giant stepwidth and current orientation is presently unknown since rounding of the steps due to thermal fluctuations, noise, and inhomogeneities in the array make it difficult to experimentally measure the actual stepwidths. This prevents us from making a *quantitative* comparison between the results of our experiments and those of theory; only a *qualitative* comparison can be made. Based on our study of the square-lattice arrays, however, we hypothesize that this relationship might be $\cos(2\theta)$ or $\cos^2(2\theta)$, where θ is the angle off the [10] orientation.

The vortex model presented in this paper provides a phenomenological explanation of why fractional giant

Shapiro steps can or cannot occur in the various types of arrays studied. The pendulum model, however, gives a detailed description of how the gauge-invariant phase differences of the individual junctions evolve per rf cycle. In this model, we see that Kirchhoff's voltage law *constrains* the evolution of the phase differences so that for the [11] square- and [2$\bar{1}$ $\bar{1}$] triangular-lattice cases, the only periodic solution allowed is one which corresponds to integer giant Shapiro steps. The perpendicular junctions in the [10]-oriented square- and [10$\bar{1}$]-oriented triangular-lattice arrays, however, allow the phase differences of the other junctions in the array to evolve more freely per rf cycle. As a result, the allowed periodic solutions correspond to both fractional and integer giant Shapiro steps.

ACKNOWLEDGMENTS

*Permanent address: Physics Department, Eastern Nazarene College, Quincy, MA 02170.

[1]S. Shapiro, Phys. Rev. Lett. **11**, 80 (1963).

[2]Ch. Leeman, Ph. Lerch, and P. Martinoli, Physica (Amsterdam) **126B**, 475 (1984); T. D. Clark, Phys. Rev. B **8**, 137 (1973).

[3]S. P. Benz, M. S. Rzchowski, M. Tinkham, and C. J. Lobb, Phys. Rev. Lett. **64**, 693 (1990).

[4]J. U. Free, S. P. Benz, M. S. Rzchowski, M. Tinkham, C. J. Lobb, and M. Octavio, Phys. Rev. B **41**, 7267 (1990).

[5]K. H. Lee, D. Stroud, and J. S. Chung, Phys. Rev. Lett. **64**, 692 (1990).

[6]H. C. Lee, D. B. Mast, R. S. Newrock, L. Bortner, K. Brown, F. P. Esposito, D. C. Harris, and J. C. Garland, Physica B **165&166**, 1571 (1990).

[7]L. L. Sohn, M. S. Rzchowski, J. U. Free, S. P. Benz, M. Tinkham, and C. J. Lobb, Phys. Rev. B **44**, 925 (1991).

[8]Similar results were also obtained by H. Eikmans and J. E. van Himbergen (unpublished) using a stability analysis.

[9]R. K. Brown and J. C. Garland, Phys. Rev. B **33**, 7827 (1986).

[10]W. Y. Shih and D. Stroud, Phys. Rev. B **30**, 6774 (1984).

[11]Similarities in magnetoresistance of [10]-oriented and [11]-oriented square-lattice arrays of *underdamped* Josephson junctions were reported by H. S. J. van der Zant, H. A. Rijken, and J. E. Mooij, J. Low Temp. Phys. **82**, 67 (1991).

[12]See Fig. 1(a) in Ref. 7.

[13]Lee *et al.* (Ref. 6) have reported seeing integer and fractional giant Shapiro steps in triangular-lattice Pb-Au Josephson-junction arrays. The orientation of the arrays studied was [10$\bar{1}$]. R. Newrock (private communication).

[14]W. C. Stewart, Appl. Phys. Lett. **10**, 277 (1968); D. E. McCumber, J. Appl. Phys. **39**, 3113 (1968).

[15]P. J. Russer, J. Appl. Phys. **43**, 2008 (1972).

[16]M. S. Rzchowski, L. L. Sohn, and M. Tinkham, Phys. Rev. B **43**, 8682 (1991).

[17]M. J. Renne and D. Polder, Rev. Phys. Appl. **9**, 25 (1974).

[18]B. D. Josephson, Phys. Lett. **1**, 251 (1962).

[19]M. Octavio, J. U. Free, S. P. Benz, R. S. Newrock, D. B. Mast, and C. J. Lobb, Phys. Rev. B **44**, 4601 (1991).

[20]C. J. Lobb, D. W. Abraham, and M. Tinkham, Phys. Rev. B **27**, 150 (1983).

[21]Simulations with periodic boundary conditions were done on 4×4, 6×6, and 8×8 junction [11]-oriented arrays. These simulations showed that the vortices disappeared and reappeared in the next-nearest-neighbor cells during one rf cycle. See Ref. 7 for more details.

[22]S. Teitel and C. Jayaprakash, Phys. Rev. B **27**, 598 (1983).

[23]The absence of fractional steps in the [11]-oriented square-lattice array at $f = \frac{1}{3}$ can also be explained by using Kirchhoff's voltage law. As opposed to the two we found in the $f = \frac{1}{2}$ state, there are actually three different types of staircases in the array at $f = \frac{1}{3}$. By Kirchhoff's voltage law, the voltage across each staircase must be the same. We again deduce that the only periodic solution which satisfies this requirement is one in which every junction must phase slip $2\pi n$ per rf cycle.

[24]We have simulated junctions whose current-phase relationship has been modified to $\sin(k\alpha) + \sin(m\alpha)$. We obtained I-V curves which show subharmonic steps corresponding to $(n/q) = 1/k$ and $(n/q) = 1/m$. It follows then that the $\sin(k\alpha)$ term contributes to the $2\pi/k$ harmonic of the time-dependent voltage and the $\sin(m\alpha)$ term, to the $2\pi/m$ harmonic.
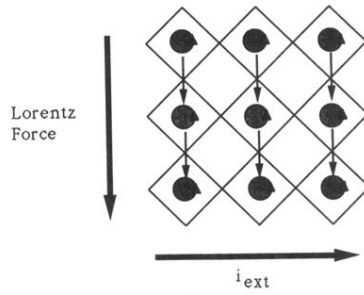
FIG. 7. Vortex configuration in the [11]-oriented square-lattice array at $f = \frac{1}{2}$. Large vertical arrow indicates the direction of the Lorentz force resulting from i_{ext}. Small arrows indicate macroscopic motion of vortices during one rf cycle on the $n/q = 1$ step.
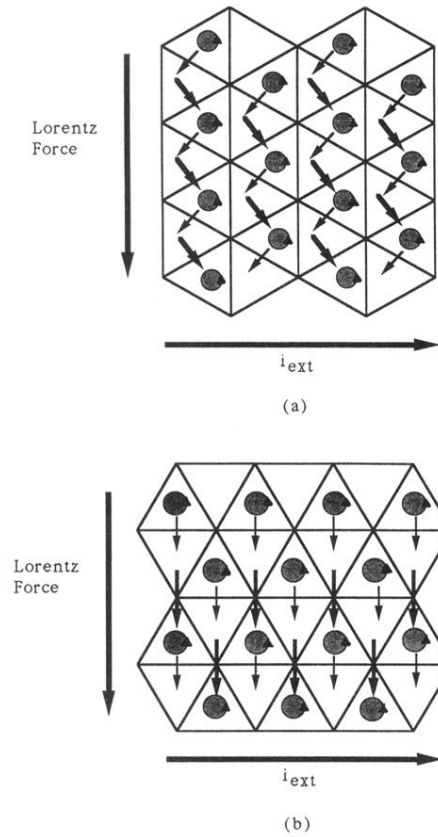
FIG. 8. Vortex configuration in the (a) $[10\bar{1}]$-oriented and (b) $[2\bar{1}\bar{1}]$-oriented triangular-lattice array at $f = \frac{1}{2}$. Again, large vertical arrow indicates the direction of the Lorentz force resulting from i_{ext}. For (a), arrows indicate macroscopic motion of vortices during 2 subsequent rf cycles on the $n/q = 1/2$ step. While the light arrows indicate vortex motion during one rf cycle, the heavy arrows indicate vortex motion during a subsequent rf cycle. For (b), light and heavy arrows show two possible vortex motions occuring sequentially in one rf cycle.